Neuroradiology (2010) 52:37–46
DOI 10.1007/s00234-009-0539-2

FUNCTIONAL NEURORADIOLOGY

Impact of fMRI-guided advanced DTI fiber tracking techniques on their clinical applications in patients with brain tumors

Raimund Kleiser · Philipp Staempfli · Anton Valavanis · Peter Boesiger · Spyros Kollias

Received: 2 February 2009 / Accepted: 13 May 2009 / Published online: 29 May 2009

Abstract
Introduction White matter tractography based on diffusion tensor imaging has become a well-accepted non-invasive tool for exploring the white matter architecture of the human brain in vivo. There exist two main key obstacles for reconstructing white matter fibers: firstly, the implementation and application of a suitable tracking algorithm, which is capable of reconstructing anatomically complex fascicular pathways correctly, as, e.g., areas of fiber crossing or branching; secondly, the definition of an appropriate tracking seed area for starting the reconstruction process. Large intersubject, anatomical variations make it difficult to define tracking seed areas based on reliable anatomical landmarks. An accurate definition of seed regions for the reconstruction of a specific neuronal pathway becomes even more challenging in patients suffering from space occupying pathological processes as, e.g., tumors due to the displacement of the tissue and the distortion of anatomical landmarks around the lesion.
Methods To resolve the first problem, an advanced tracking algorithm, called advanced fast marching, was applied in this study. The second challenge was overcome by combining functional magnetic resonance imaging (fMRI) and diffusion tensor imaging (DTI) in order to perform fMRI-guided accurate definition of appropriate seed areas for the DTI fiber tracking. In addition, the performance of the tasks was controlled by a MR-compatible power device.
Results Application of this combined approach to eight healthy volunteers and exemplary to three tumor patients showed that it is feasible to accurately reconstruct relevant fiber tracts belonging to a specific functional system.
Conclusion fMRI-guided advanced DTI fiber tracking has the potential to provide accurate anatomical and functional information for a more informed therapeutic decision making.

Keywords Diffusion tensor imaging · Fiber tracking · fMRI · Tumor

Raimund Kleiser and Philipp Staempfli contributed equally to this work.

R. Kleiser · P. Staempfli · A. Valavanis · S. Kollias
Institute of Neuroradiology, University Hospital Zurich,
Frauenklinikstrasse 10,
8091 Zürich, Switzerland

P. Staempfli · P. Boesiger
Institute for Biomedical Engineering, University and ETH Zurich,
Zürich, Switzerland

R. Kleiser (✉)
Oö. Gesundheits- und Spitals-AG, Institute of Radiology,
Landes-Nervenklinik Wagner-Jauregg,
Wagner-Jauregg-Weg 15,
4020 Linz, Austria
e-mail: raimund.kleiser@gespag.at

Introduction

Diffusion tensor imaging (DTI) [3, 31] is a promising, non-invasive magnetic resonance imaging (MRI) method for studying non-invasively the anatomical organization of major white matter fiber systems (for a review, see [27]). In the last years, the technique of diffusion-weighted imaging has been increasingly applied in clinical routine, e.g., in management of acute stroke [19, 20, 36, 44] or in the characterization of multiple sclerosis lesions [8, 25, 33, 34]. A topic, which currently is receiving increased attention, is the application of DTI and DTI fiber tracking in the investigation of patients with intracranial tumors. One of the first publications by Witwer et al. [48] demonstrated

displaced fiber tracks on directionally color-coded maps. Goebells et al. showed different fractional anisotropy (FA) values in the center as compared to the periphery of gliomas as well as, in the adjacent normal appearing white matter. They also found differences in FA ratios between low- and high-grade tumors [11, 12]. Helton et al. [14] investigated the feasibility of DTI to visualize and quantify white matter tract involvement in pontine tumors.

Accurate preoperative localization and visualization of the displaced or infiltrated fiber tracts in relation to intracranial tumors is crucial for treatment planning [15, 50] and potentially for the postoperative prognosis. Therefore, new developments aim at presurgical, intraoperative, and follow-up postsurgical applications of DTI to provide relevant information related to the tumor affected tissue [1, 23, 29]. Functional MRI (fMRI)-driven fiber tracking methods are the most recent clinical application in this direction [35, 39]. Guye et al. applied the basic fast marching tracking algorithm [30] in order to perform fMRI-driven fiber tracking [13]. Thereby, probabilistic connectivity maps of healthy subjects were computed and compared with a map of a patient suffering from a tumor.

A key obstacle for accurate reconstruction of neuronal fibers is the selection of a suitable tracking algorithm. In certain areas of the white matter, such as the corona radiata or the occipital white matter where an abundant crossing and/or merging of different fiber systems takes place, the main diffusion intravoxel direction does not necessarily correspond to the main fiber direction. This is due to the tensor's voxel averaged quantity and the limited resolution of available DTI acquisitions [5, 17, 45]. Consequently, simple tracking algorithms, which incorporate only the main diffusion direction for determining the propagation pathway (or track), are not adequate in such anatomically complex areas, and the reconstructed trajectories are often compromised by the wrong directional information [4, 17, 18, 21, 22, 42, 45]. Recently, sophisticated tracking algorithms have been developed to overcome these limitations particularly to ameliorate tracking results in crossing and branching situations [24, 30, 38, 46, 47, 51]. In the present study, this problem was addressed by using a tracking algorithm called "advanced fast marching" (aFM), which has been specifically developed [38] in order to improve reconstruction of white matter trajectories in anatomically complex areas. The quality of the aFM algorithm was evaluated and compared with other tracking algorithm by reconstructing different neuronal fiber systems and networks in the human brain [40, 41].

Another main issue in the field of DTI-based fiber tractography is the definition of a tracking seed region that would be appropriate for the reconstruction of white matter tracts relevant to a specific functional system or network. If seed areas are slightly misplaced by only a few voxels, the reconstructed trajectories may represent tracks from different white matter fiber systems. Intersubject anatomical variations make it difficult to define tracking seed areas based merely on reliable anatomical landmarks, even in brains of healthy subjects. This problem becomes more difficult in the presence of a space occupying intracranial pathological processes, as, e.g., tumor, where the definition of functionally relevant tracking seed regions based on anatomical landmarks becomes more challenging due to displacement or infiltration of the surrounding tissue and a potential reorganization of involved functional systems. To overcome this second obstacle, a combined approach of DTI and fMRI is presented where seed areas for the DTI tracking algorithm are defined based on fMRI activation patterns specific to individual patient. For the fMRI acquisitions, a new powerful setup was developed, which allowed real-time monitoring and recording of the executed task performance for future evaluation steps. This information is also useful in regard to the comprehension of the progressive course of disease. In the present study, these new combined techniques are applied in healthy volunteers and exemplary in patients with intracranial tumors to demonstrate the feasibility of fMRI-guided, DTI fiber tracking in combination with advanced tracking algorithms and its potential impact in clinical applications.

Materials and methods

Data were acquired from eight healthy, right-handed volunteers and three right-handed patients. The study was approved by the local ethics committee (EK: 09–2006(ETH)). To demonstrate the clinical feasibility of the methodological approach, three patients suffering from intracranial tumors of different histology (a low-grade glioma, a high-grade glioma, and a meningioma) located in the vicinity of the central sulcus and, therefore, expected to affect the primary motor cortex (see Fig. 1 for a detailed depiction of the tumor localization) were selected. All measurements were performed on a 3-T, whole-body MRI system (Philips Achieva, Best, the Netherlands), equipped with 80 mT/m/ms gradient coils and an eight-element receive head coil array (MRI Devices, Waukesha, USA). Each imaging session consisted of a high resolution T_1-weighted anatomical scan, a DTI scan, and two fMRI scans.

Anatomical data were obtained with a 3D T_1-weighted turbo field-echo scan consisting of 220 interleaved slices in sagittal orientation with the following parameters: field of view (FOV)=230×230 mm^2, slice thickness=1.5 mm, slice gap=−0.75 mm, resulting in an effective slice thickness of 0.75 mm, acquisition matrix=256×256 pixels, repetition time (TR)=20 ms, echo time (TE)=2.3 ms, flip angle (FA)=20°, number of signal averages (NSA)=1.

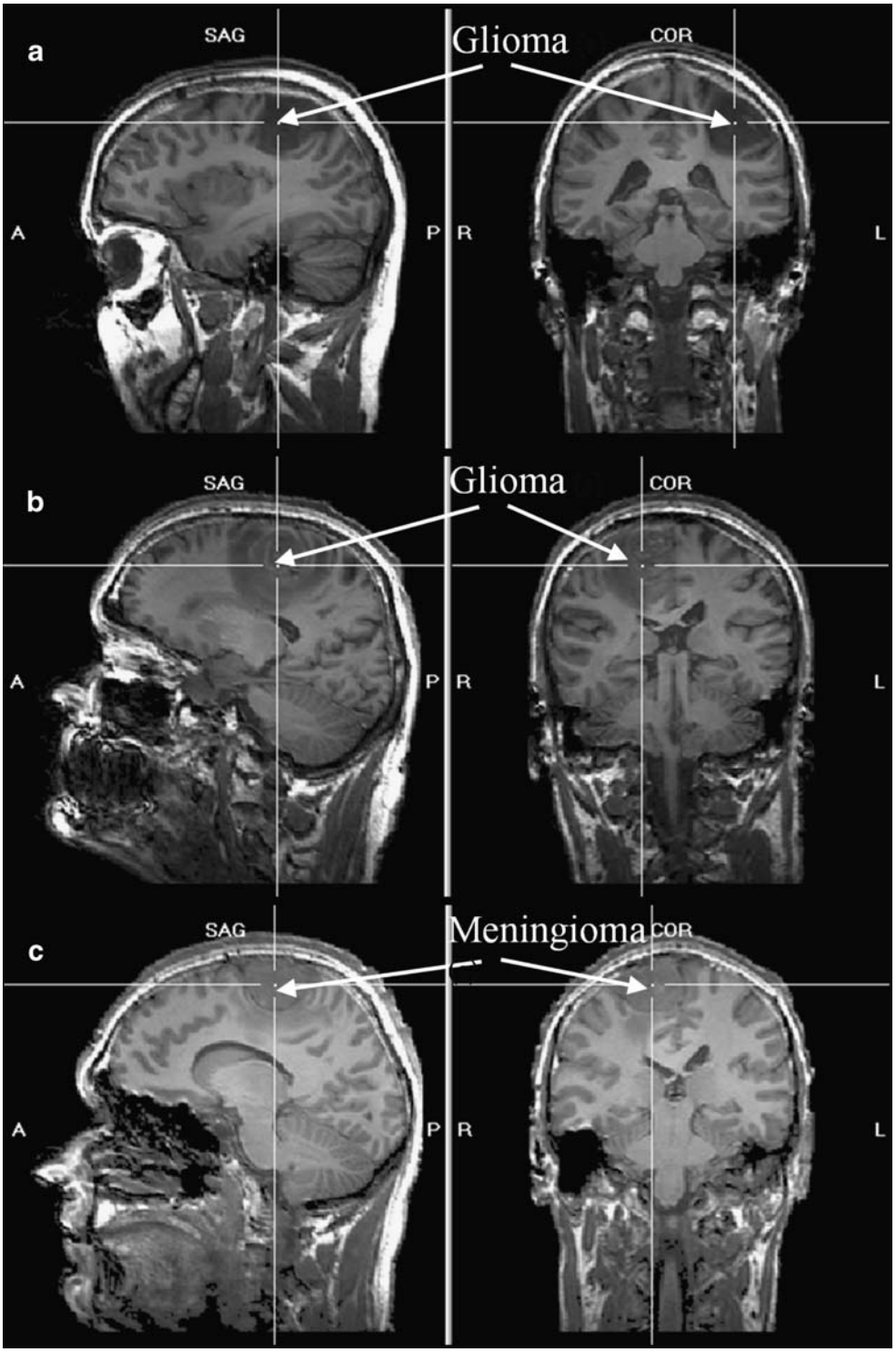

Fig. 1 Localization of the tumors (indicated by the *white cross-hairs* and *white arrows*) on sagittal (*left column*) and coronal (*right column*) slices. Patient **a** suffered from a postcentral, low-grade glioma; **b** from a precentral, high-grade glioma; and **c** from an extra-axial meningioma compressing the precentral gyrus and the paracentral lobule

The sequence most commonly used for DTI is spin-echo single-shot echo planar imaging (SE-sshEPI) [31] due to its motion insensitivity and relatively high SNR. Thus, for the DTI scan, a whole brain diffusion-weighted SE-sshEPI sequence was applied with the following parameters: FOV=220×220 mm^2, matrix=96×96 pixels, reconstructed to 128×128 pixels, 60 contiguous slices, slice thickness=2.0 mm, TE=50 ms, NSA=2, 60% partial k-space acquisition. Diffusion weighting with a maximal *b* factor of 1,000 s/mm^2 was carried out along 15 icosahedral directions [6], complemented by one scan with *b*=0. A 2.1-fold sensitivity encoding (SENSE) reduction factor [32] was applied in order to reduce susceptibility artifacts and thus to enhance image quality [2, 16].

The fMRI series consisted of two whole brain gradient-echo EPI sequences (30 slices, field of view=220×220 mm^2, matrix=80×80 pixels, reconstructed to 128×128 pixels, slice thickness=4.0 mm, TR=3,000 ms, TE=35 ms, SENSE factor=2.0). In order to facilitate the registration process, we selected exactly a factor of two between the DTI and the fMRI slice thickness, i.e., DTI slice thickness was 2.0 mm and fMRI slice thickness 4.0 mm. Thus, each fMRI slice overlapped in each case with exactly two DTI data slices. Each fMRI acquisition consisted of seven blocks of 30 s motor activity alternating with seven blocks of 30 s rest, resulting in a total acquisition time of 7 min. In the active phase, a previously practiced power grip task with a frequency of about 0.5 Hz had to be executed with each hand separately and clearly below the individual maximal force. So, it was possible to keep the force constant during the entire session. The MR-compatible power grip device was connected to an external laptop. This setup allowed to monitor and record the signal from the motor grip device in real time (Fig. 2) and to analyze the task performance (as, e.g., frequency, amplitude, and regularity) offline after the scan session. The sampling rate was 500 Hz. The frequency of the motor task and the mean power of the signal for both hands were determined separately. Furthermore, a laterality index (LI=$(x_{right}-x_{left})/(x_{right}+x_{left})$) was calculated to describe a potential laterality of the right or left hand in regard to frequency or power, in particular in the patient group. Thereby, −1 corresponds to a one-sided left-handed value and + 1 to a pure right-handed value.

The analysis of the fMRI data was performed with SPM2 (SPM2; Wellcome Department of Cognitive Neurology, London, UK). A detailed overview of fMRI analysis is given by Frackowiak et al. [9]. After correcting the fMRI images for interscan motion artifacts, the data were smoothed (without prior spatial normalization) with a Gaussian filter (kernel=5 mm). A temporal cut-off of 128 s was applied to remove low-frequency drift artifacts. Data from each run were then modeled using the general linear model with separate delayed boxcar functions. Multiple comparison correction was applied using the false discovery rate method (FDR $p<0.05$ with cluster level >20) [10]. The mean EPI image and the SPM{t} map of the fMRI scan were coregistered to the b0 image of the DTI scan using the coregister algorithm of SPM. The result of the coregistration was visually verified (comparing, e.g., contour differences) and showed a very good special agreement of the two dataset.

In the DTI data, eddy-current-induced image warping was reduced with a correlation-based 3D-affine registration algorithm [28]. The independent elements of the diffusion tensor were obtained on a voxel-by-voxel basis using singular value decomposition. After diagonalization of the diffusion tensor, the eigenvalues and eigenvectors were determined [26]. All these DTI related calculations, subsequent fiber tracking, and the statistical evaluation of the fiber tracks were performed using a dedicated in-house software package written in C++.

Tracking was initiated in 3D-seed-areas computed on the basis of the activation patterns detected in the fMRI as follows: the centers of gravity of the fMRI activations weighted with the significance level in the primary motor cortex of both hemispheres were determined; due to the fact that fMRI activations are located within gray matter, the centers of gravity were enlarged spherically (radius=7 mm) to define 3D seed areas within the adjacent white matter; from these areas, DTI fiber tracking was performed for each hemisphere separately. Thereby, the aFM algorithm [38] was applied. In this study, the aFM algorithm was executed with 70,000 time steps. For reconstructing the fibers a 10% voxel connectivity was used. The fractional anisotropy stop criterion was defined as 0.2. One fiber reconstruction with these parameters took about 45 s on a standard PC. Finally, the cortico-spinal fibers were selected, and the mean fractional anisotropy (FA) values of all voxels intersected by these fibers were derived. Additionally, in the patient

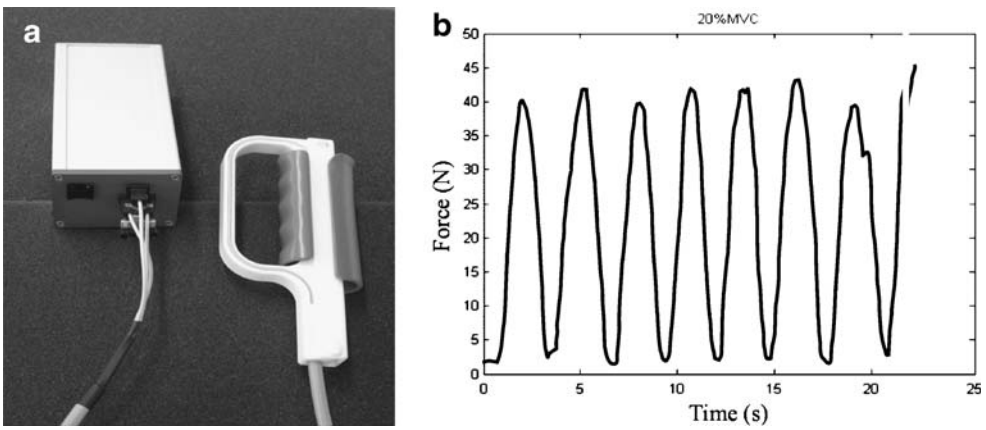

Fig. 2 **a** MR-compatible grip device with laptop connector box used for the hand motor task. **b** Recorded signal, which served as real-time monitoring for ensuring correct task performance, was analyzed offline (frequency, amplitude, and regularity) following the scan session

data, seed areas were placed manually around the tumor in order to investigate the effects of the tumor not only on the cortico-spinal tract but also on the fiber integrity and architecture of the entire adjacent white matter.

Results

Findings in the healthy volunteers and the patients' behavior data sets

Offline quantitative analysis of the motor performance using the power grip device showed that the range of the laterality indices of frequency in the healthy group was between −0.152 and 0 with a mean of −0.047, and the range of power was between −0.142 and 0.087 with a mean of 0.002 (Fig. 3). So, the motor task was executed slightly faster with the left hand than with the right one. This difference was quite small and probably is a reflection of greater difficulty to maintain a constant frequency of grasping with the non-dominant left hand since all subjects were right-handed. With regard to the power between the right and the left hand, no statistical significant differences could be found (paired *t* test). The healthy group executed the task with the same good performance for both hands. The laterality indices of the patients were also in the range

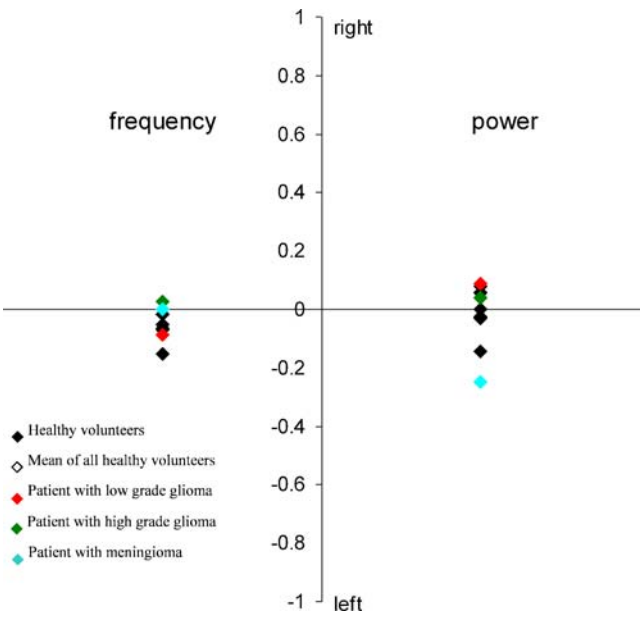

Fig. 3 The performance of healthy subjects and patients during the motor task. The laterality index $(x_{right}-x_{left})/(x_{right}+x_{left})$ describes any tendency of the frequency or power of the recorded signal to the left (−1) or right (+1) hand. For the eight healthy volunteers (*black dots*, some of them are overlapping) as well as for all three patients (*red*, *green*, and *blue dots*), both values are around 0. So, task performance was similar for the left and the right hand

of the healthy group (patient 1: frequency −0.088/power 0.089; patient 2: frequency 0.027/power 0.038; patient 3: frequency 0/power −0.248). Surprisingly, the presence of the tumor in all three patients did not affect their motor output performance.

Findings in the healthy volunteers MR data sets

Figure 4 illustrates reconstructed fibers in a data set of one healthy volunteer. The red areas are the tracking seed regions within the left and right primary motor cortex, derived from the fMRI activations. It shows fiber reconstructions calculated by the aFM algorithm. It is important to mention that reproducible fiber pathways were reconstructed in all other subjects, and similar results were achieved in every volunteer data set. Thereby, the aFM algorithm reconstructed reliably fibers of the cortico-spinal tract in all healthy subjects within both hemispheres, as anatomically expected. As a comparison, the fiber reconstruction was also performed with the FACT algorithm [27]. Fifty fiber reconstructions were started from randomly calculated positions within every voxel of the seed region with the FACT algorithm. The stepsize was defined as 0.3 mm, whereby trilinear interpolation for calculating the new propagating direction was applied in every integration step. The fractional anisotropy stop criterion was defined as 0.2. Thereby, in most of the datasets, all fibers were deviated from the seed region into U-fibers or other main fiber bundles. In most cases, no cortico-spinal connections could be reconstructed by the FACT algorithm. A detailed comparison between the aFM and FACT algorithm is published by Staempfli et al. [40, 41]. It could be shown that a standard tracking algorithm like the FACT is not able to resolve complex fiber situations like crossing or kissing.

The FA values of all voxels, which are intersected by the cortico-spinal fibers in each subject, are depicted in the plot in Fig. 5 (the black dots represent the values of the healthy volunteers). Thereby, fibers of both hemispheres were examined separately. On the vertical-axis, the mean FA values for the right hand (and thus for the cortico-spinal fibers within the left hemisphere) are recorded. On the horizontal axis, the FA values for the left hand (and thus for the cortico-spinal fibers within the right hemisphere) are registered. No laterality is detectable, and all FA values vary a small range between 0.48 and 0.60 with a mean FA value of 0.53 for the left and a mean FA value of 0.56 for the right hand (indicated by the white dot).

Findings in the patients MR data sets

Figure 6 depicts fiber reconstructions in the data sets of the three tumor patients. Figure 6a, c, and d illustrates the 3D seed areas and the bilaterally reconstructed tracks, generat-

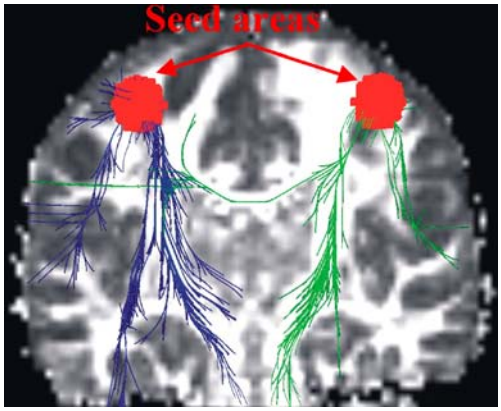

Fig. 4 Estimated tracts calculated by the aFM algorithm in a representative healthy volunteer. Tracking was initiated in the motor cortex within the fMRI-evoked seed areas (*red spheres*, indicated by the *red arrows*). The reconstructed fibers correspond to the left and right cortico-spinal connections

ed with the same technique as in the volunteer data: In all three patient data sets, the hemispheric location of the tracking seed areas is quite asymmetric due to the space occupying effect of the tumor. As visible, e.g., in Fig. 6a on the left side, the tumor displaced the region around the cortical hand area and pushed it superior. Nevertheless, as in the volunteer data, the aFM algorithm reconstructed reliably fibers of the cortico-spinal tract in all patient data sets.

The asymmetries between the healthy and the tumor affected hemisphere are also evident in Fig. 6b, where fibers from a large seed area placed in the centrum semiovale of the white matter were reconstructed for preoperative planning purposes, resulting in reconstruction of several projectional, commissural, and association fiber systems (this reconstruction is done with a conventional algorithm, not with the aFM). In order to reduce the number of resulting fibers, one single fiber reconstruction was started from every voxel within the seed region with the FACT algorithm. All other parameters of the algorithm were left unchanged and defined as described above. The resulting reconstructions should give an overall overview of the effect of the glioma in white matters adjacent to the tumor. It demonstrates inferior displacement of the long association fiber system represented by the superior longitudinal fasciculus and medial displacement of the peripheral callosal fibers and the projectional cortico-spinal tract, whereas no fibers are visible within the tumor mass. Similar images have been obtained in the other two patient data sets for preoperative planning.

The fractional anisotropy values of the displaced cortico-spinal tracts showed similar values to those of the contra-lesional hemisphere in all patients. Furthermore, the values were in the same range as the values from the healthy volunteers. The FA values of the left and right tracts in all three patients are also shown in Fig. 5 and are marked as colored dots. All values, both of the healthy volunteers and patient data group, are in the same range, and no statistically significant differences between tumor patients and healthy subjects were found.

Discussion

In this study, the technique of fMRI-based DTI fiber tracking is applied in a clinical setting with tumor patient data. Thereby, fMRI information is used for defining functionally related structures as accurate start regions for subsequent fiber tracking. The additional information provided by fMRI is important considering the large intersubject anatomical variations of the human brain, particularly in the presence of a space occupying pathological process affecting the spatial position of anatomical landmarks. Thus, the results illustrate that fMRI-guided DTI fiber tracking allows to identify tracking start regions reliably based on functional anatomy rather than solely on anatomical landmarks as well in healthy volunteers as in tumor patients. Furthermore, the study demonstrates that DTI benefits from the combination with fMRI in order to reconstruct fibers related to specific functional areas. In cases of

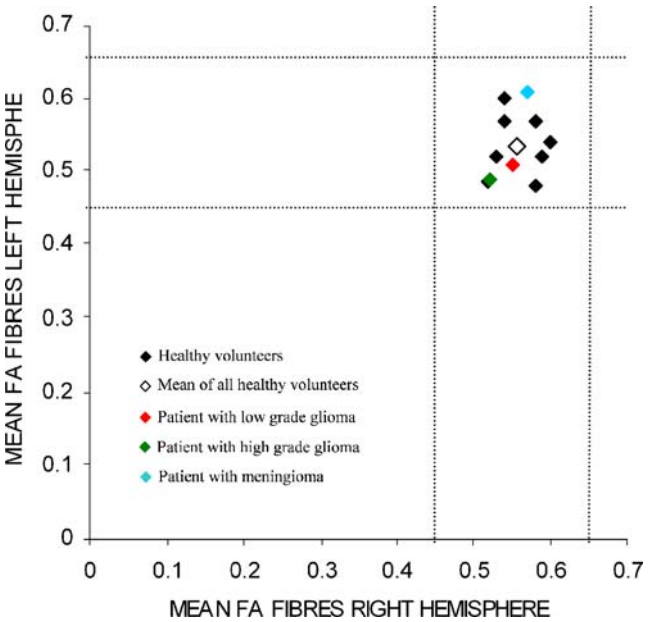

Fig. 5 FA values of all voxels intersected by the reconstructed cortico-spinal tracts for both hemispheres of the eight healthy volunteers and the three tumor patients. On the *x*-axis, the mean FA values for the left hand (i.e., for the cortico-spinal tract in the right hemisphere), and on the *y*-axis, the FA values for the right hand (i.e., for the cortico-spinal tract in the left hemisphere)

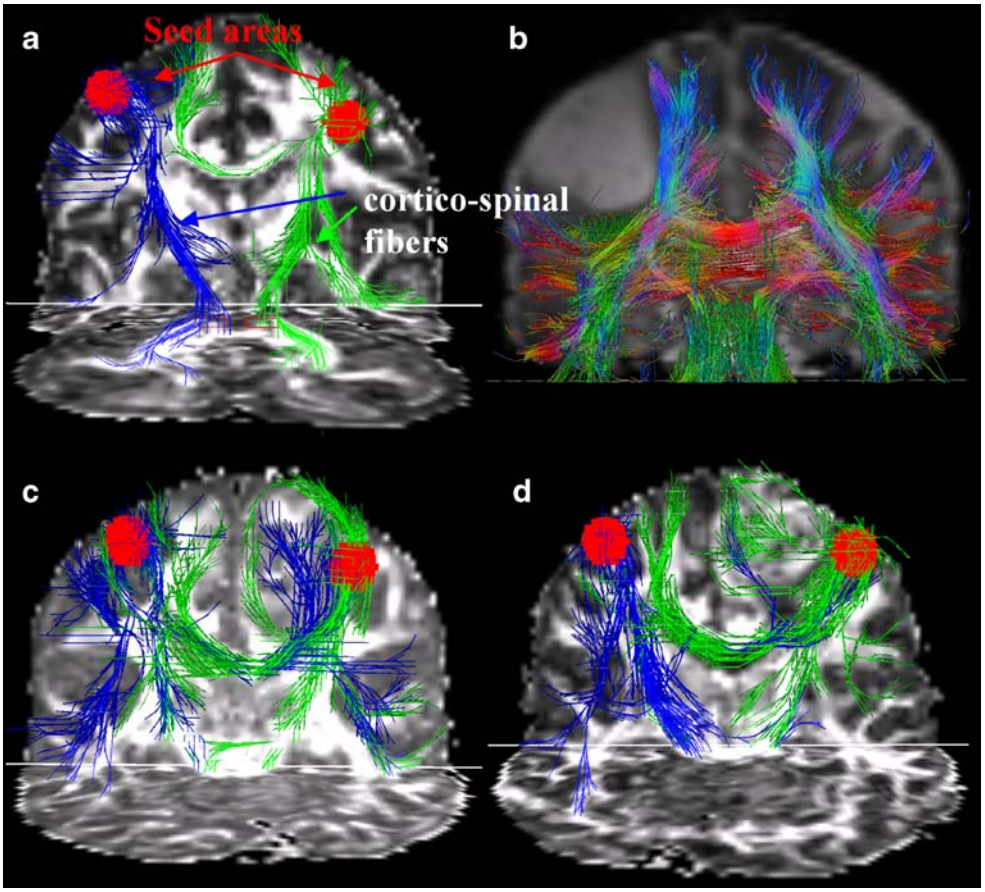

Fig. 6 Tracking results in the patient data sets. **a** and **b** depict results of the patient harboring a parietal low-grade glioma, **c** from the patient suffering from a central high-grade glioma, and **d** from the patient with a frontal convexity meningioma. In **a**, **c**, and **d**, the asymmetric, displaced tracking seed areas (*red spheres*) in the motor cortex and the reconstructed fibers from these areas are depicted (calculated by the aFM algorithm). In **b**, fibers from a large seed area, covering the entire white matter in the coronal slice, were reconstructed to give an overview of the effects of the tumor on the major fiber systems of the white matter

intracranial tumors, the fMRI approach compliments and enhances the accuracy of DTI information for preoperative planning by defining the relevant functionally related structures as accurate start regions for fiber tracking with advanced tracking techniques. This is crucial in complex areas like the (motor)cortex region where many different neuronal systems are tightly packed, especially in the presence of tumors [7]. If start regions are slightly shifted in this area, the combined fMRI/DTI approach can prevent from the obstacle of estimating completely different fiber systems, which might belong to the target system.

Additionally, and in contrast to publications with similar approaches [37, 43], it has been demonstrated that the possibility to supervise in real time the performance of the power task using the MR-compatible grip device for the fMRI examination serves two important points. Firstly, the supervision gives a real-time feedback about the volunteer's or patient's task performance during the actual scanning. This allows, e.g., repeating a session immediately in case of any compliance problems related to the correct task execution by the patient. Even more important, based on the recorded task signal, quantitative measures, e.g., frequency and power and a resulting laterality index, can be established. The index allows a quantitative estimation of the tumor effects on motor output as compared to the non-affected hemisphere. This information is potentially useful for monitoring motor recovery and also postoperative functional outcome not only in tumors but also in several pathological processes that may affect the sensorimotor network. In the present preliminary study, we could show that none of the different types of tumors examined affected the patient's motoric capabilities related to the specific grasping task. It remains to be further explored whether this quantification may provide additional relevant information in differentiating between tumor infiltration and tumor displacement. Our preliminary experience indicates that the motor output and clinical behavior obtained by the grip device strongly correlate with the FA values measured with DTI.

In order to define the fMRI-based tracking seed regions, a center of gravity approach weighted with the significance level was applied in this study. Therefore, center of gravity with the significant values of the fMRI activation was calculated. On the one hand, this approach accounts for different distributions of fMRI clusters, which is, e.g., important when considering a situation with an fMRI activation consisting of two or more almost equally activated clusters. On the other hand, it inherently incorporates the information of the most significantly activated

fMRI voxels due to the fact that highly activated voxels contribute most to the final determination of the center of gravity.

In contrast to a recent publication [35], we did not find statistically significant differences in the FA values of the cortico-spinal fibers between the healthy control group and the three tumor patients. This may indicate that all three tumors displaced the cortico-spinal fibers without significant fiber compression or tumor infiltration, which would change the anisotropic properties of the adjacent white matter despite the fact that one of the tumors was a high-grade glioma. This hypothesis is in analogy with the equivalent, excellent motor performance of all three patients. This assumption is further supported by the fact that there were no differences in the measured motor-task fMRI signal between the healthy and affected hemisphere, and none of the three patients showed or reported any abnormal motor behavior during grasping. This may indicate structural integrity of the cortico-spinal tracts within both hemispheres, which is in analogy with the findings of the DTI analysis. This hypothesis is further supported by intraoperative observations as reported by Yasargil [49] according to which both low- and high-grade gliomas in their initial and intermediate growth phases usually displace the peritumoral projectional, commissural, and associational fiber bundles but do not invade or transect them.

The complementary information provided by fMRI and DTI provides a quantitative estimate related to both the structural integrity of the white matter and the functional status of the interconnected relevant cortical areas that may be displaced or infiltrated by the tumor. This information can be used not only to enhance presurgical planning and intra-surgical decision making but also to predict postoperative functional outcome and thus improve patient counseling. Thereby, the effort to acquire the additional information is negligible for the patient, as demonstrated in this study. The DTI scan can be acquired in a few more scan minutes in the same scan session in which all the other necessary images for the surgery are acquired (anatomical and fMRI data). The data processing is performed offline with dedicated software packages without involvement of the patient. Thus, an integration of the proposed technique can be done without any changes of the patient treatment.

Future development should aim at enlarging our experience with various histological types of well-localized tumors in order to be able to derive statistical and clinical relevant correlations between the fMRI/DTI findings and the motor status of the patient. This is prerequisite for drawing conclusions related to the potential of this approach for differentiating between white matter displacement and tumor infiltration. The range of application is not limited to the motor system, which was used exemplary to describe the method. The sensory, visual, and semantic system are further interesting areas for this method. From the methodological point of view, an important task is to further improve tracking reliability at the boundary between gray and white matter due to the inherent low anisotropy of the gray matter. This could be achieved by increasing both spatial resolution and diffusion sensitivity during data acquisition. Diffusion sensitivity, higher spatial resolution, and consequently an increase of data quality will gain from the transition to higher static magnetic field strengths.

In conclusion, the presented imaging approach holds great promise for better understanding of the structural/functional relationship of the human brain in physiological conditions and its reorganizational changes in the presence of disease. It is expected that the combined fMRI/DTI quantitative approach will have a great clinical impact for providing improved pre- and intrasurgical decision making and will enhance the accuracy of postsurgical outcome prediction for better patient counseling.

Acknowledgments The authors are grateful for the continuing support of Philips Medical Systems and the financial support by the Strategic Excellence Project Program (SEP) of the ETH Zurich.

Conflict of interest statement We declare that we have no conflict of interest.

References

1. Arfanakis K, Gui M, Lazar M (2006) Optimization of white matter tractography for pre-surgical planning and image-guided surgery. Oncol Rep 15:1061–1064
2. Bammer R, Auer M, Keeling SL, Augustin M, Stables LA, Prokesch RW, Stollberger R, Moseley ME, Fazekas F (2002) Diffusion tensor imaging using single-shot SENSE-EPI. Magn Reson Med 48:128–136. doi:10.1002/mrm.10184
3. Basser PJ, Mattiello J, LeBihan D (1994) MR diffusion tensor spectroscopy and imaging. Biophys J 66:259–267. doi:10.1016/S0006-3495(94)80775-1
4. Basser PJ, Pajevic S (2000) Statistical artifacts in diffusion tensor MRI (DT-MRI) caused by background noise. Magn Reson Med 44:41–50. doi:10.1002/1522-2594(200007)44:1<41::AID-MRM8>3.0.CO;2-O
5. Basser PJ, Pajevic S, Pierpaoli C, Duda J, Aldroubi A (2000) In vivo fiber tractography using DT-MRI data. Magn Reson Med 44:625–632. doi:10.1002/1522-2594(200010)44:4<625::AID-MRM17>3.0.CO;2-O
6. Batchelor PG, Atkinson D, Hill DL, Calamante F, Connelly A (2003) Anisotropic noise propagation in diffusion tensor MRI sampling schemes. Magn Reson Med 49:1143–1151. doi:10.1002/mrm.10491
7. Beisteiner R, Lanzenberger R, Novak K, Edward V, Windischberger C, Erdler M, Cunnington R, Gartus A, Streibl B, Moser E, Czech T, Deecke L (2000) Improvement of presurgical patient evaluation by generation of functional magnetic resonance risk maps. Neurosci Lett 290:13–16. doi:10.1016/S0304-3940(00)01303-3
8. Filippi M, Cercignani M, Inglese M, Horsfield MA, Comi G (2001) Diffusion tensor magnetic resonance imaging in multiple sclerosis. Neurology 56:304–311
9. Frackowiak RSJ, Friston KJ, Frith C (2004) Human brain function. Academic, New York

10. Genovese CR, Lazar NA, Nichols T (2002) Thresholding of statistical maps in functional neuroimaging using the false discovery rate. Neuroimage 15:870–878. doi:10.1006/nimg.2001.1037
11. Goebell E, Fiehler J, Ding XQ, Paustenbach S, Nietz S, Heese O, Kucinski T, Hagel C, Westphal M, Zeumer H (2006) Disarrangement of fiber tracts and decline of neuronal density correlate in glioma patients—a combined diffusion tensor imaging and 1H-MR spectroscopy study. AJNR Am J Neuroradiol 27:1426–1431
12. Goebell E, Paustenbach S, Vaeterlein O, Ding XQ, Heese O, Fiehler J, Kucinski T, Hagel C, Westphal M, Zeumer H (2006) Low-grade and anaplastic gliomas: differences in architecture evaluated with diffusion-tensor MR imaging. Radiology 239:217–222. doi:10.1148/radiol.2383050059
13. Guye M, Parker GJ, Symms M, Boulby P, Wheeler-Kingshott CA, Salek-Haddadi A, Barker GJ, Duncan JS (2003) Combined functional MRI and tractography to demonstrate the connectivity of the human primary motor cortex in vivo. Neuroimage 19:1349–1360. doi:10.1016/S1053-8119(03)00165-4
14. Helton KJ, Phillips NS, Khan RB, Boop FA, Sanford RA, Zou P, Li CS, Langston JW, Ogg RJ (2006) Diffusion tensor imaging of tract involvement in children with pontine tumors. AJNR Am J Neuroradiol 27:786–793
15. Inoue T, Ogasawara K, Beppu T, Ogawa A, Kabasawa H (2005) Diffusion tensor imaging for preoperative evaluation of tumor grade in gliomas. Clin Neurol Neurosurg 107:174–180. doi:10.1016/j.clineuro.2004.06.011
16. Jaermann T, Crelier G, Pruessmann KP, Golay X, Netsch T, van Muiswinkel AM, Mori S, van Zijl PC, Valavanis A, Kollias S, Boesiger P (2004) SENSE-DTI at 3 T. Magn Reson Med 51:230–236. doi:10.1002/mrm.10707
17. Jones DK (2003) Determining and visualizing uncertainty in estimates of fiber orientation from diffusion tensor MRI. Magn Reson Med 49:7–12. doi:10.1002/mrm.10331
18. Jones DK, Basser PJ (2004) "Squashing peanuts and smashing pumpkins": how noise distorts diffusion-weighted MR data. Magn Reson Med 52:979–993. doi:10.1002/mrm.20283
19. Karonen JO, Liu Y, Vanninen RL, Ostergaard L, Kaarina Partanen PL, Vainio PA, Vanninen EJ, Nuutinen J, Roivainen R, Soimakallio S, Kuikka JT, Aronen HJ (2000) Combined perfusion- and diffusion-weighted MR imaging in acute ischemic stroke during the 1st week: a longitudinal study. Radiology 217:886–894
20. Karonen JO, Vanninen RL, Liu Y, Ostergaard L, Kuikka JT, Nuutinen J, Vanninen EJ, Partanen PL, Vainio PA, Korhonen K, Perkio J, Roivainen R, Sivenius J, Aronen HJ (1999) Combined diffusion and perfusion MRI with correlation to single-photon emission CT in acute ischemic stroke. Ischemic penumbra predicts infarct growth. Stroke 30:1583–1590
21. Lazar M, Alexander AL (2003) An error analysis of white matter tractography methods: synthetic diffusion tensor field simulations. Neuroimage 20:1140–1153. doi:10.1016/S1053-8119(03)00277-5
22. Lazar M, Alexander AL (2005) Bootstrap white matter tractography (BOOT-TRAC). Neuroimage 24:524–532. doi:10.1016/j.neuroimage.2004.08.050
23. Lazar M, Alexander AL, Thottakara PJ, Badie B, Field AS (2006) White matter reorganization after surgical resection of brain tumors and vascular malformations. AJNR Am J Neuroradiol 27:1258–1271
24. Lazar M, Weinstein DM, Tsuruda JS, Hasan KM, Arfanakis K, Meyerand ME, Badie B, Rowley HA, Haughton V, Field A, Alexander AL (2003) White matter tractography using diffusion tensor deflection. Hum Brain Mapp 18:306–321. doi:10.1002/hbm.10102
25. Maldjian JA, Grossman RI (2001) Future applications of DWI in MS. J Neurol Sci 186(Suppl 1):S55–S57. doi:10.1016/S0022-510X(01)00494-4
26. Mori S, Barker PB (1999) Diffusion magnetic resonance imaging: its principle and applications. Anat Rec 257:102–109. doi:10.1002/(SICI)1097-0185(19990615)257:3<102::AID-AR7>3.0.CO;2-6
27. Mori S, van Zijl PC (2002) Fiber tracking: principles and strategies - a technical review. NMR Biomed 15:468–480. doi:10.1002/nbm.781
28. Netsch T, vanMuiswinkel A (2004) Quantitative evaluation of image-based distortion correction in diffusion tensor imaging. IEEE Trans Med Imaging 23:789–798. doi:10.1109/TMI.2004.827479
29. Nimsky C, Ganslandt O, Hastreiter P, Wang R, Benner T, Sorensen AG, Fahlbusch R (2005) Preoperative and intraoperative diffusion tensor imaging-based fiber tracking in glioma surgery. Neurosurgery 56:130–137 discussion 138
30. Parker GJM, Wheeler-Kingshott CAM, Barker GJ (2002) Estimating distributed anatomical connectivity using fast marching methods and diffusion tensor imaging. IEEE Trans Med Imaging 21:505–512. doi:10.1109/TMI.2002.1009386
31. Pierpaoli C, Jezzard P, Basser PJ, Barnett A, Di Chiro G (1996) Diffusion tensor MR imaging of the human brain. Radiology 201:637–648
32. Pruessmann KP, Weiger M, Scheidegger MB, Boesiger P (1999) SENSE: sensitivity encoding for fast MRI. Magn Reson Med 42:952–962. doi:10.1002/(SICI)1522-2594(199911)42:5<952::AID-MRM16>3.0.CO;2-S
33. Rovaris M, Bozzali M, Iannucci G, Ghezzi A, Caputo D, Montanari E, Bertolotto A, Bergamaschi R, Capra R, Mancardi GL, Martinelli V, Comi G, Filippi M (2002) Assessment of normal-appearing white and gray matter in patients with primary progressive multiple sclerosis: a diffusion-tensor magnetic resonance imaging study. Arch Neurol 59:1406–1412. doi:10.1001/archneur.59.9.1406
34. Rovaris M, Gallo A, Valsasina P, Benedetti B, Caputo D, Ghezzi A, Montanari E, Sormani MP, Bertolotto A, Mancardi G, Bergamaschi R, Martinelli V, Comi G, Filippi M (2005) Short-term accrual of gray matter pathology in patients with progressive multiple sclerosis: an in vivo study using diffusion tensor MRI. Neuroimage 24:1139–1146. doi:10.1016/j.neuroimage.2004.10.006
35. Schonberg T, Pianka P, Hendler T, Pasternak O, Assaf Y (2006) Characterization of displaced white matter by brain tumors using combined DTI and fMRI. Neuroimage 30:1100–1111. doi:10.1016/j.neuroimage.2005.11.015
36. Schwamm LH, Koroshetz WJ, Sorensen AG, Wang B, Copen WA, Budzik R, Rordorf G, Buonanno FS, Schaefer PW, Gonzalez RG (1998) Time course of lesion development in patients with acute stroke: serial diffusion- and hemodynamic-weighted magnetic resonance imaging. Stroke 29:2268–2276
37. Smits M, Vernooij MW, Wielopolski PA, Vincent AJ, Houston GC, van der Lugt A (2007) Incorporating functional MR imaging into diffusion tensor tractography in the preoperative assessment of the corticospinal tract in patients with brain tumors. AJNR Am J Neuroradiol 28:1354–1361. doi:10.3174/ajnr.A0538
38. Staempfli P, Jaermann T, Crelier GR, Kollias S, Valavanis A, Boesiger P (2006) Resolving fiber crossing using advanced fast marching tractography based on diffusion tensor imaging. Neuroimage 30:110–120. doi:10.1016/j.neuroimage.2005.09.027
39. Staempfli P, Jaermann T, Valavanis A, Boesiger P, Kollias S (2004) fMRI based fiber tracking using SENSE-DTI at 3 Tesla. Presented at Proc Intl Soc Magn Reson Med, Kyoto, Japan, 2004.
40. Staempfli P, Reischauer C, Jaermann T, Valavanis A, Kollias S, Boesiger P (2008) Combining fMRI and DTI: a framework for exploring the limits of fMRI-guided DTI fiber tracking and for verifying DTI-based fiber tractography results. Neuroimage 39:119–126. doi:10.1016/j.neuroimage.2007.08.025
41. Staempfli P, Rienmueller A, Reischauer C, Valavanis A, Boesiger P, Kollias S (2007) Reconstruction of the human visual system based on DTI fiber tracking. J Magn Reson Imaging 26:886–893. doi:10.1002/jmri.21098
42. Tournier JD, Calamante F, King MD, Gadian DG, Connelly A (2002) Limitations and requirements of diffusion tensor fiber tracking: an assessment using simulations. Magn Reson Med 47:701–708. doi:10.1002/mrm.10116

43. Upadhyay J, Ducros M, Knaus TA, Lindgren KA, Silver A, Tager-Flusberg H, Kim DS (2007) Function and connectivity in human primary auditory cortex: a combined fMRI and DTI study at 3 Tesla. Cereb Cortex 17:2420–2432. doi:10.1093/cercor/bhl150
44. Warach S, Dashe JF, Edelman RR (1996) Clinical outcome in ischemic stroke predicted by early diffusion-weighted and perfusion magnetic resonance imaging: a preliminary analysis. J Cereb Blood Flow Metab 16:53–59. doi:10.1097/00004647-199601000-00006
45. Watts R, Liston C, Niogi S, Ulug AM (2003) Fiber tracking using magnetic resonance diffusion tensor imaging and its applications to human brain development. Ment Retard Dev Disabil Res Rev 9:168–177. doi:10.1002/mrdd.10077
46. Weinstein D, Kindlmann G, Lundberg E (1999) Tensorlines: advection-diffusion based propagation through diffusion tensor fields. IEEE Visualisation:249–253.
47. Westin CF, Maier SE, Mamata H, Nabavi A, Jolesz FA, Kikinis R (2002) Processing and visualization for diffusion tensor MRI. Med Image Anal 6:93–108. doi:10.1016/S1361-8415(02)00053-1
48. Witwer BP, Moftakhar R, Hasan KM, Deshmukh P, Haughton V, Field A, Arfanakis K, Noyes J, Moritz CH, Meyerand ME, Rowley HA, Alexander AL, Badie B (2002) Diffusion-tensor imaging of white matter tracts in patients with cerebral neoplasm. J Neurosurg 97:568–575
49. Yasargil MG (1994) CNS tumors. Thieme Medical, New York
50. Yu CS, Li KC, Xuan Y, Ji XM, Qin W (2005) Diffusion tensor tractography in patients with cerebral tumors: a helpful technique for neurosurgical planning and postoperative assessment. Eur J Radiol 56:197–204. doi:10.1016/j.ejrad.2005.04.010
51. Zhang S, Bastin ME, Laidlaw DH, Sinha S, Armitage PA, Deisboeck TS (2004) Visualization and analysis of white matter structural asymmetry in diffusion tensor MRI data. Magn Reson Med 51:140–147. doi:10.1002/mrm.10673